Probability Hypothesis Density-Based Multitarget Tracking With Bistatic Range and Doppler Observations

Martin Tobias and Aaron D. Lanterman
School of Electrical and Computer Engineering
Georgia Institute of Technology
Atlanta, Georgia 30332–0250 U.S.A.
E-mail: mtobias@ece.gatech.edu, lanterma@ece.gatech.edu

Abstract

Ronald Mahler's Probability Hypothesis Density (PHD) provides a promising framework for the passive coherent location of targets observed via multiple bistatic radar measurements. We apply a particle filter implementation of the Bayesian PHD filter to target tracking using both range and Doppler measurements from a simple non-directional receiver that exploits non-coöperative FM radio transmitters as its "illuminators of opportunity". Signal-to-noise ratios, probabilities of detection and false alarm and bistatic range and Doppler variances are incorporated into a realistic two-target scenario. Bistatic range cells are used in calculating the birth particle proposal density. The tracking results are compared to those obtained when the same tracker is used with range-only measurements. This is done for two different probabilities of false alarm. The PHD particle filter handles ghost targets well and has improved tracking performance when incorporating Doppler measurements along with the range measurements. This improved tracking performance, however, comes at the cost of requiring more particles and additional computation.

I. Introduction

A. The PHD and Passive Radar

A particle filter implementation of a multitarget tracker, based on Mahler's Probability Hypothesis Density (PHD) [1]–[3], was first applied to passive radar in a rudimentary fashion in [4]. Having shown promising results, the implementation was expanded to incorporate a

realistic passive radar configuration in [5]. However, only range measurements were considered. This paper presents an improved version of the PHD-based particle filter as applied to passive coherent location, and we incorporate Doppler measurements into the PHD-based particle filter, thus effecting a range and velocity multitarget tracker. We compare its tracking performance to that of the range-only tracker when used in a realistic scenario.

The remainder of this section provides a brief review of multitarget, multisensor tracking, followed by a review of finite-set statistics (FISST), which is used to derive the PHD-based multitarget Bayesian filter. In Section II, the concept of passive coherent location[1] is reviewed. Section III describes the simulation configuration, while Section IV presents the PHD particle filter implementation. A review of the radar parameters used is contained in Section V, and the results of the simulation are in Section VI. A summary of conclusions is found in Section VII.

B. Review of Multitarget, Multisensor Tracking

The theory of single-sensor, single-target tracking is rather well understood. The workhorse of such systems is the ubiquitous extended Kalman filter, along with its Interacting Multiple Model (IMM) extension. The newer unscented Kalman filters [6] and fully nonlinear, non-Gaussian algorithms, such as particle filters [7]–[9], are becoming popular as well [10].

When multiple targets are present,[2] however, the situation becomes rapidly more complex. It is not known which reports from a given sensor are created by which targets. The complexity increases when multiple sensors are used, and things become even more problematic in the presence of false alarms and missed detections.

1) Association-Based Multitarget Tracking: Most mainstream tracking algorithms have historically been based on the idea that there is some true report-to-track association that must be estimated. Common techniques may involve "soft" report-to-track assignments, as found in Joint Probabilistic Data Association (JPDA) [13], or "hard" assignments, as performed in Multiple Frame Assignment (MFA) using Lagrangian relaxation techniques [12], [14]–[19].

[1]To the best of our knowledge, the term "passive coherent location" was coined by Dick Lodwig of Lockheed Martin (then, IBM) and his colleagues.

[2]When multiple targets are first mentioned in a paper, authors usually cite Blackman's classic book [11]. Instead, we recommend the more recent, vastly expanded, and incredibly thorough (over 1200 pages) tome by Blackman and Popoli [12].

2) Multitarget Tracking without Explicit Associations: Some alternatives to the association-based multitarget, multisensor tracking algorithms are slowly gaining attention [10]. In these alternative approaches, no explicit association between tracks and targets are made. Proponents of such techniques contend that estimated associations, like those of hard and soft report-to-track, are both unnecessary and potentially misleading. One novel approach that avoids explicit associations is the Symmetric Measurement Equation [20]–[23] method developed by Kamen and colleagues in the early 1990's. Another approach, which is the focus of this paper, is based on finite-set statistics (FISST).

C. Finite-Set Statistics

Mathematically speaking, a real-valued random variable is a function that maps elements of an underlying probability space into the space of real numbers. In most engineering applications, one can forget about this fundamental definition and deal directly with concepts related to the random variable, such as probability density functions, cumulative distribution functions, moments, entropy, etc. Extending the notion to random vectors, such as the state vectors in single-target tracking systems, is straightforward. Further extension to random "processes", which map elements of an underlying probability space to the space of functions defined on a continuum, is much more complex. However, the final results are readily employed by engineers.

In an extensive series of conference papers (particularly the SPIE sessions on *Signal and Data Processing of Small Targets* and *Signal Processing, Sensor Fusion, and Target Recognition*), Mahler has proposed "random sets", which map elements of an underlying probability space to sets, as the most natural framework to address data fusion in general and target tracking systems in particular. Unfortunately, the probability theory associated with random sets is nowhere near as well-known as the theory associated with the more mundane random variables and vectors. However, the presentation of the theory in the book by Goodman, Mahler, and Nguyen [24] is thorough. The authors define "set integrals" and "set derivatives" in terms of generalised Radon-Nikodým derivatives. These set generalisations of calculus allow for generalisations of probability densities and distribution functions. Once the random sets are given a solid measure-theoretic foundation, ideas from statistics, such as maximum-likelihood estimation and maximum a-posteriori estimation, and from information theory, such as entropy and Kullback-Leibler distances, can be extended to these random sets (see Sections 5.2 and 5.3 of [24]).

Mahler [25], [26] attempts to distill random set theory to nuts-and-bolts principles that practicing engineers can easily apply. One of the more elegant aspects of traditional Kalman filtering is the way in which the prior and posterior distributions are characterised by a small set of sufficient statistics that are easily propagated in the Kalman recursion. When target tracking is generalised to the multitarget, multisensor scenario, however, no simple analogous implementation seems to appear.

Nevertheless, attempting to replicate the simplicity of the Kalman filter for the multitarget, multisensor case, Mahler and Zajic [27] propose propagating the first moment of a function that maps a set of targets into a continuous function space. This functional mapping is essential since the expectation of a set-valued random variable is not well-defined. They choose a function that places Dirac deltas at the target positions and call its first moment a Probability Hypothesis Density (PHD). The PHD acts much like an intensity of a Poisson point process; in fact, it is the first factorial moment density found in point process theory [2], [28]. Like the mean and variance of the Kalman filter, the PHD is readily propagated forward through the Bayesian prediction and data update steps. It is, of course, a bit more complicated since an entire function is being propagated forward, not just a mean vector and a covariance matrix.

II. Passive Coherent Location (PCL)

A. Range

Consider a bistatic radar consisting of a passive receiver and an independent transmitting antenna. If the direct path signal is measured along with the reflected path signal, then correlation processing yields the following range measurement observation:

$$R = \sqrt{(x - x_t)^2 + (y - y_t)^2} + \sqrt{(x - x_r)^2 + (y - y_r)^2} \tag{1}$$

where (x_r, y_r) and (x_t, y_t) are the locations of the antennas, and (x, y) is the location of the target. Thus, a target can be located along an ellipse, where the receiver and transmitter are located at the foci of the ellipse.

It is difficult to build highly directional receiver antennas that operate at the low frequencies of interest in a passive radar system that exploits FM broadcasts. Hence, rather than exploit angle-of-arrival information to resolve a target's location, multiple transmitter-receiver pairs are employed instead. The target can thus be located at the intersection of the resulting bistatic range ellipses. This is not to imply that angle information, if available in a PCL system, is

of no value; we simply wish to explore the limits of what can be achieved without it. Future work will study the effect of including angle information.

A problem that arises, however, is that of ghost targets. A ghost target appears at the intersection of bistatic range ellipses where no target is present. This is due to the nature of the ellipse geometry and confuses multitarget trackers, which must process ghost targets until they disappear. Noisy measurements exacerbate the problem. The PHD-based particle filter, however, is seen to adequately handle ghost targets with no additional conceptual effort, i.e., no explicit ghost-busting[3] logic is needed.

B. Velocity

By observing the Doppler shift caused by the target in the received signal's frequency, a bistatic radar also provides the rate of change of the range measurement given in (1):

$$\dot{R} = \frac{(x-x_r)\dot{x} + (y-y_r)\dot{y}}{\sqrt{(x-x_r)^2 + (y-y_r)^2}} + \frac{(x-x_t)\dot{x} + (y-y_t)\dot{y}}{\sqrt{(x-x_t)^2 + (y-y_t)^2}} \tag{2}$$

With $\dot{R}$ measurements from multiple transmitter-receiver pairs, a target's velocity components $(\dot{x}, \dot{y})$ can be found.

III. Scenario Configuration

Our demonstration scenario is the same as that in [5]. The Field of View (FoV) consists of an 80 km $\times$ 80 km stretch of the Washington D.C. area. The receiving antenna is in the middle of the FoV and is assumed to be located on one of the Lockheed Martin Mission Systems buildings. A receiver such as Lockheed Martin's *Silent Sentry*® system, except with a simpler antenna, is assumed. The illuminators of opportunity consist of three non-coöperative FM transmitters. The transmitter specifications are given in Table I, and their locations can be seen in Figure 1(a). The receiver coördinates and system specifications are listed in Table II. All antennas are assumed to be omni-directional, and thus they have unity gain. The noise figure listed, which is meant to account for external interference sources as well as internal receiver noise, is assumed to be a valid approximation for an urban environment such as Washington D.C. [29].

[3]See the following website for a description of a ghost-busting technique: http://www.clw.org/nmd/businessweek.html

TABLE I

TRANSMITTING ANTENNA SPECIFICATIONS.

Call Letters	Latitude	Longitude	Frequency (f)	Power (P_T)	Bandwidth (β)
WAMU	38.936 °N	77.093 °W	88.5 MHz	50.0 kW	45 kHz
WETA	38.892 °N	77.132 °W	90.9 MHz	75.0 kW	45 kHz
WPGC	38.864 °N	76.911 °W	95.5 MHz	50.0 kW	45 kHz

TABLE II

RECEIVER SYSTEM SPECIFICATIONS.

Latitude	39.153 °N
Longitude	77.215 °W
Coherent Processing Interval (CPI)	0.5 sec
Reference Temperature (T_0)	290 K
Noise Figure (NF)	30 dB
Gain (G_R)	0 dB

IV. THE PHD-BASED PARTICLE FILTER

Ronald Mahler introduced the concept of a Probability Hypothesis Density (PHD), which is defined as being any function that, when integrated over any given area, specifies the expected number of targets present in that area. More specifically, the PHD is the factorial moment density found in point process theory [2], [28], and it provides a straightforward method of estimating the number of targets in a region under observation. We thus expect the PHD to be a useful tool for tracking multiple targets, especially in handling the many ghost targets that arise from noisy bistatic radar measurements. Using probability generating functionals and set calculus, Mahler derives Bayesian time-update and data-update equations that use the PHD, respectively, to perform motion prediction and incorporate sensor observations [2], [3], [27], [30], [31]. This allows the multitarget tracker to incorporate both range and Doppler observation information, which we expect to produce better tracking results than using range-only information.

We use the particle filter implementation of the update equations [32], whereby the PHD is represented by a collection of particles and their corresponding weights. At time-step k,

each particle in the filter is a vector of the form $\xi_i = [x_i \ y_i \ \dot{x}_i \ \dot{y}_i]^T$ and has a weight $w_{i,k}$, where (x_i, y_i) specify the particle's location and $(\dot{x}_i, \dot{y}_i)$ specify its velocity components. As per the defining property of the PHD,

$$\tilde{N} = E[no.\ of\ targets] = [N_{k|k}]_{nearest\ integer} \tag{3}$$

where

$$N_{k|k} = \sum_i w_{i,k} \tag{4}$$

A. Initialisation

The simulation begins by independently and randomly assigning the particles' x and y components to fall within the FoV. The $\dot{x}$ and $\dot{y}$ components are independently and randomly chosen to be between a minimum of -495 km/h and a maximum of 495 km/h (i.e., -137.5 m/s to 137.5 m/s), where North and East are positive. The particle weights are initialised to zero, since we do not expect any targets to be present at time $k = 0$.

B. Time Update

The time-update step of the particle filter involves multiplying each particle vector by a simple constant-velocity transition matrix and adding Gaussian process noise. This propagates the particles forward in time, thus modelling the target motion, where each time step k of simulation represents one second of time.

To model the PHD of new targets that appear in the FoV, birth particles are added to the simulation during the time-update step. They indicate where new targets are likely to appear at the current time step. To economise on the number of particles needed in the simulation and to achieve better target tracking results, we propose a targeted cluster placement of birth particles to be used wherever a bistatic range ellipse intersects with the edge of the FoV. At the location of the intersection, a cluster of birth particles is centred and spread independently in both x and y according to a normal distribution with a standard deviation equal to a bistatic range cell (see Section V-E and Table III). When no bistatic range ellipses intersect the FoV boundaries, the birth particles are randomly placed uniformly in a 9 km-wide band around the inside edge of the FoV.

In both placement methods, the velocity components of the particles are initialised independently and randomly with uniform probability over all possible velocities, as given in Section IV-A. However, if a particle is placed in the right-hand quadrant of the FoV, then its

initial $\dot{x}$ component is restricted to negative values. If it is placed in the left-hand quadrant, then the $\dot{x}$ component is initialised to positive values only. A similar restriction is enforced on the initial $\dot{y}$ component of a particle that is placed in either the top or bottom quadrants of the FoV.

The simulation assumes that targets will not spontaneously disappear and that they will not spawn new targets. Any particles, whose x and y components place them outside of the FoV, have their location components adjusted, so that they are repositioned in a mirror-image fashion across the nearest FoV edge back into the FoV. This keeps all of the particles inside the region of interest.

We now weight the particles according to the method described in [33] for particle filter representations of the PHD. Since we simply use the prior target-motion model to propagate the particles from the previous time step, these propagated particles maintain the same weights as they had at the end of the previous time step. The birth particles, when the uniform placement method is used, are given equal weighting. When the targeted cluster placement is used, however, the birth particles are given weights

$$\tilde{w}_{birth_{i,k+1}} = \frac{1}{J_{k+1} \cdot Q_x \cdot q_x(x_{i,k+1}|z_{k+1}) \cdot Q_y \cdot q_y(y_{i,k+1}|z_{k+1})} \tag{5}$$

where J_{k+1} is the number of birth particles used and $q_x(x_{i,k+1}|z_{k+1})$ and $q_y(y_{i,k+1}|z_{k+1})$ are normal density functions with means equal, respectively, to the x and y positions of the ellipse intersection at the FoV edge and with standard deviations equal to the intersection's corresponding bistatic range cell. Q_x is set to 2, if the intersection occurs along the left or right edge of the FoV, and is set to 1, otherwise. Similarly, if the intersection occurs along the top or bottom edges, then Q_y is set to 2; otherwise, it is set to 1. This takes into account the doubling of particle density due to the folding-in of particles found outside the FoV.

In both birth particle placement methods, we normalise the birth particle weights, such that $\sum \tilde{w}_{birth_{i,k+1}}$ equals the expected number of new targets per scan. Since we assume that only one target might enter the FoV at each time step, we set this term equal to one. However, one could choose a higher or lower value if an alternative birth model is desired. This step is not explicitly mentioned in [33], but we found this normalisation necessary to have the particle filter accurately represent the PHD.

The results of the time-update step are the propagated and birth particles and their associated weights, indicated by $\tilde{w}_{i,k+1}$, which represent the predicted PHD for time-step $k+1$.

C. Data Update

In the data-update step, the time-predicted $\tilde{w}_{i,k+1}$ are converted to the final PHD particle weights, $w_{i,k+1}$, by incorporating the radar range and Doppler observations at time $k+1$. Given a single sensor with the set of observations $Z_s = \{z_1, \ldots, z_m\}$ made at time $k+1$, probability of detection $p_D(\boldsymbol{\xi})$, single-target likelihood function $f(\mathbf{z}|\boldsymbol{\xi})$ and Poisson-distributed false alarms with parameter λ and density $c(\mathbf{z})$, the data-updated weights are computed by

$$w_{i,k+1} = (\sum_{n=1}^{m} u_{i,n}) \ + \ \tilde{w}_{i,k+1}(1 - p_D(\boldsymbol{\xi})) \tag{6}$$

where

$$u_{i,n} = \frac{p_D(\xi_i) f(z_n|\xi_i) \tilde{w}_{i,k+1}}{\lambda c(z_n) \ + \ \sum_{j=1}^{N} p_D(\xi_j) f(z_n|\xi_j) \tilde{w}_{j,k+1}} \tag{7}$$

for $i = 1, \ldots, N$, where N is the total number of particles.

The set of observations Z_s contains both range and Doppler measurements. Thus, either $f_R(z_n|\xi_i)$ or $f_{\dot{R}}(z_n|\xi_i)$ must be used as the single-target likelihood function $f(z_n|\xi_i)$, depending on whether z_n is a range or a Doppler observation, respectively. The computations of $p_D(\boldsymbol{\xi})$, $f(\mathbf{z}|\boldsymbol{\xi})$, λ and $c(\mathbf{z})$ are given in Section V.

In the bistatic radar case, each receiver and transmitter pair constitutes a "sensor". In our example, there are three sensors in the configuration, and three sets of range and Doppler observations are collected at each time step, namely $\{Z_1, Z_2, Z_3\}$. Following a procedure suggested by Mahler [34] to determine the final weights for this multisensor case, (6) and (7) are first applied to Z_1. The resulting $w_{i,k+1}$ are then used as the $\tilde{w}_{i,k+1}$ to reiterate (6) and (7) over Z_2. The latter procedure is repeated for Z_3 to find the final multisensor particle weights. The order in which the observation sets are processed does affect the final result; although, practically, it has little effect. This issue remains available for further investigation.

Having generated the final particle weights, $w_{i,k+1}$, the expected number of targets in the FoV is computed via (3). The locations of the $\tilde{N}$ expected targets are found by extracting the $\tilde{N}$ highest peaks from the PHD represented by these weights. We currently use an expectation-maximisation algorithm for this extraction.

D. Peak Extraction

To find the target locations and their velocities, the $\tilde{N}$ highest peaks must be extracted from the PHD. To find these peaks, we assume that the PHD in the neighbourhood of the peaks

can be approximated by Gaussian distributions, so we attempt to fit a mixture of Gaussians to the PHD using an expectation-maximisation (EM) algorithm [35], which we modify to account for the particle weights. Thus, the algorithm to find $\theta_g = (\alpha_g, \mu_g, \Sigma_g)$, which are the weight, mean and covariance parameters of the g-th Gaussian distribution in the mix, is given by the following iteration:

Expectation:

$$P(g|x_i) = \frac{p(x_i|\theta_g)\alpha_g}{\sum_{j=1}^{G} p(x_i|\theta_j)\alpha_j} \tag{8}$$

Maximisation:

$$\alpha_g^{new} = \sum_{i=1}^{N} w_i P(g|x_i) \tag{9}$$

$$\mu_g^{new} = \frac{1}{\alpha_g^{new}} \sum_{i=1}^{N} w_i P(g|x_i) x_i$$

$$\Sigma_g^{new} = \frac{1}{\alpha_g^{new}} \sum_{i=1}^{N} w_i P(g|x_i)(x_i - \mu_g^{new})(x_i - \mu_g^{new})^T$$

where $p(x_i|\theta_j)$ is a normal density function with mean μ_j and covariance matrix Σ_j, G is the number of Gaussians in the mixture and $G \geq \tilde{N}$, where $\tilde{N}$ is the number of targets estimated by integrating the PHD via (3).

The μ_g are initialised by randomly choosing G particles and selecting their components to be the values for the μ_g. To obtain good results from the EM algorithm [36], short runs of the algorithm are performed, and the run that produces the highest likelihood is then used for a longer EM run. The result is the final estimate of the G-Gaussian mixture. When iterating the EM algorithm, a run is terminated upon achieving a given threshold or if a covariance matrix becomes singular. The preceding is performed multiple times for different values of G, and a minimum description length (MDL) criterion is then used to select the best fitting Gaussian mixture by maximising the penalised likelihood [37]:

$$L(\mathbf{x}; \theta_G) - \frac{\rho}{2} \ln N \tag{10}$$

where $\rho = (G-1) + G(d + d(d+1)/2)$ and d is the particle dimensionality (in the current case, $d = 4$), and where

$$L(\mathbf{x}; \theta_G) = \frac{N}{\sum w_i} \sum_{i=1}^{N} w_i \ln \sum_{j=1}^{G} \alpha_j p(x_i|\theta_j) \tag{11}$$

The means of the $\tilde{N}$ highest-weighted Gaussians in the best fitting mixture are then taken to be the expected locations and velocities of the targets. A benefit of using the EM algorithm is that it produces covariance matrices that provide one with a measure of uncertainty in the location and velocity estimates.

E. Resampling

Before iterating the particle filter over the next time step, the particles are resampled via a Monte Carlo method to obtain an initial number (i.e., the amount before birth particles were added) of equally weighted particles where

$$\sum_i w_i = \sum_i w_{i,k+1} \tag{12}$$

V. Bistatic Radar Variables

A. Signal-to-Noise ratio, SNR

To compute $f(\mathbf{z}|\boldsymbol{\xi})$ and $p_D(\boldsymbol{\xi})$, it is first necessary to compute each sensor's signal-to-noise ratio for each particle. The SNR of a particle is calculated as follows [38]–[40]:

$$\text{SNR}(\xi_i) = \frac{K}{R_T^2 R_R^2} \tag{13}$$

where R_T and R_R are the distances between the particle's (x, y) location and the sensor's transmitting and receiving antennas, respectively, and

$$K = \frac{P_T\, G_T\, G_R\, \lambda_f^2\ \sigma_{rcs}\, F_T^2 F_R^2}{(4\pi)^3 k\, T_0 (\frac{1}{CPI})(NF)} \tag{14}$$

where $\lambda_f = \frac{c}{f}$, c is the speed of light, and f is the frequency of the FM signal given in Table I. The transmitter power P_T is also taken from Table I, and the transmitter gain G_T is assumed to be unity. The receiver gain G_R, reference temperature T_0, coherent processing interval CPI and noise figure NF are taken from Table II. Boltzmann's constant is represented by k, and F_T and F_R are the signal propagation factors. For this study, it is assumed that signal propagation gains and losses are negligible; including such effects is planned for future work. The target's bistatic radar cross section is denoted by σ_{rcs}. All targets in the simulation are assumed to have $\sigma_{rcs} = 10$ dBsm.

B. Probability of Detection, p_D

The calculation of the bistatic radar's probability of detection is based on its SNR and the probability of false alarm, p_{FA}. At low frequencies, a target may reasonably be assumed to be slowly fluctuating; hence, a Rician target model is employed. Thus, [41]

$$p_D(\boldsymbol{\xi}) = Q\left[\sqrt{2\,\text{SNR}(\boldsymbol{\xi})}\,, \sqrt{2\ln\left(\frac{1}{p_{FA}}\right)}\,\right] \tag{15}$$

where Q is the Marcum Q-function, SNR($\boldsymbol{\xi}$) is given by (13), and p_{FA} is set to a fixed value. For a fixed p_{FA}, a gain in SNR corresponds to an increase in p_D.

In the simulation, the p_{FA} is initially set to 10^{-4}. This achieves a $p_D = 0.9999$ with an SNR $= 14.94$ dB, and a $p_D = 0.1$ when SNR $= 6.19$ dB [41]. For reasonable simulation, p_D is restricted to a maximum value of 0.99999.

Note that the $p_D(\boldsymbol{\xi})$ in (6) does not depend on any specific radar observation, since the $(1 - p_D(\boldsymbol{\xi}))$ term deals with potential missed targets. Thus, a σ_{rcs} must be chosen that one would expect a potential missed target to have were the radar to detect it. For illustration, we escape this vexing chicken-and-egg situation by choosing $\sigma_{rcs} = 10$ dBsm, since this is the value assumed in generating the simulated data.

C. Single-Target Likelihood, $f(\mathbf{z}|\boldsymbol{\xi})$

1) Range Likelihood, $f_R(\mathbf{z}|\boldsymbol{\xi})$: The single-target range likelihood function of each bistatic radar antenna pair determines how close each particle's (x, y) values are to the observed target location, given that the radar observes the range measurement given by (1). Each particle's corresponding bistatic range measurement is computed (R_{ξ_i}), as well as the difference between it and the observed range.

$f_R(z_i|\xi_i)$ is a normal density function with mean R_{ξ_i} and variance σ_r^2, where σ_r^2 is the variance of the bistatic range:

$$\sigma_r^2 = \sigma_t^2 \cdot c^2 \tag{16}$$

and [42]

$$\sigma_t^2 = \frac{1}{2\,\beta^2\,\text{SNR}(\xi_i)} \tag{17}$$

where β is the transmitter bandwidth specified in Table I, and SNR(ξ_i) is given by (13).

2) Doppler Likelihood, $f_{\dot{R}}(\mathbf{z}|\boldsymbol{\xi})$: The single-target Doppler likelihood function of each bistatic radar pair determines how close the $\dot{R}$ value of each particle, given by substituting the particle's components into (2), is to the observed $\dot{R}$ measurement. Each particle's corresponding rate of bistatic range change is computed ($\dot{R}_{\xi_i}$), as well as the difference between it and the observed $\dot{R}$.

$f_{\dot{R}}(z_i|\xi_i)$ is a normal density function with mean $\dot{R}_{\xi_i}$ and variance $\sigma_{\dot{r}}^2$, where $\sigma_{\dot{r}}^2$ is the variance of the rate of change in bistatic range:

$$\sigma_{\dot{r}}^2 = \sigma_f^2 \cdot \lambda_f^2 \tag{18}$$

where λ_f is the frequency of the transmitted signal, and [39], [40]

$$\sigma_f^2 = \max\left[\frac{3}{2\,\mathrm{SNR}\cdot(\pi\cdot CPI)^2}\ ,\ \frac{1}{CPI^2}\right] \tag{19}$$

On the right-hand side of (19), the first term in the $\max$ function is the accuracy with which the bistatic radar is able to measure the received signal. The second term is the resolution obtained from the passive radar's use of the discrete Fourier transform to compute the Doppler shift of the signal. Thus, the variance in the $\dot{R}$ measurement is the worse, i.e. greater, of the two terms.

D. False Alarm Parameters, λ and $c(\mathbf{z})$

The false alarm Poisson-distribution parameter λ is computed based on the number of range and Doppler cells present in the simulation. These, in turn, are based on the extent of range and Doppler in the scenario, as well as the bistatic range and Doppler resolutions of the radar.

Each transmitter-receiver pair's λ parameter is calculated in the following manner:

$$\lambda = (total\ no.\ cells) \times p_{FA} \tag{20}$$

where

$$total\ no.\ cells = (no.\ range\ cells) \times (no.\ Doppler\ cells) \tag{21}$$

and

$$no.\ range\ cells = \frac{range\ extent}{bistatic\ range\ resolution} \tag{22}$$

$$no.\ Doppler\ cells = \frac{Doppler\ extent}{Doppler\ resolution} \tag{23}$$

and

$$bistatic\ range\ resolution = \frac{c}{\beta} \tag{24}$$

$$Doppler\ resolution = \frac{1}{CPI} \tag{25}$$

and

$$range\ extent \;=\; 1.5 \times \sqrt{(80\text{km})^2 + (80\text{km})^2} \tag{26}$$

$$Doppler\ extent \;=\; 2\left(\frac{2V_{max}}{\lambda_f}\right) \tag{27}$$

where V_{max} is the maximum possible target velocity. The range extent value of (26) is for the hypothetical case where the receiver is located at the centre of the FoV, the transmitter is located in a corner of the FoV, and the target is located at the opposite corner. The Doppler extent found in (27) takes into account both positive and negative velocities. Thus, both extents are chosen to be as large as theoretically possible in our scenario.

The false alarms are assumed to be uniformly distributed over the range and Doppler extents, and thus the spatial distribution parameter is determined in the following manner:

$$c(\mathbf{z}) = \frac{1}{(range\ extent) \times (Doppler\ extent)} \tag{28}$$

E. Bistatic Range Cells

To place the birth particles correctly in the targeted clustering method described in Section IV-B, the size of the bistatic range cell at the cluster's location must be computed. A bistatic range cell is the resolution at which a bistatic radar can pinpoint a target's location. It is approximated by [38]:

$$\Delta R_B \approx \frac{c\tau}{2\cos(\frac{\psi}{2})} \tag{29}$$

where τ is the compressed pulse width and ψ is the bistatic angle:

$$\psi = \cos^{-1}\left[\frac{R_T^2 + R_R^2 - L^2}{2R_R R_T}\right] \tag{30}$$

where L is the distance between the transmitter and the receiver. Thus,[4]

$$\begin{aligned} \Delta R_B &\approx \frac{c\tau\sqrt{R_R R_T}}{\sqrt{(R_T + R_R)^2 - L^2}} \\ &= \frac{c\sqrt{R_R R_T}}{\beta\sqrt{(R_T + R_R)^2 - L^2}} \end{aligned} \tag{31}$$

[4]This is a correction to the derivation found in [5].

VI. SIMULATION

The simulation contains two targets. The first enters at time $k = 7$ at location (80 km, 20 km) on the East edge of the FoV and travels at -395 km/h (i.e., 109.7 m/s West). The second enters at time $k = 9$ from location (50 km, 0 km) on the South edge and travels North at 340 km/h (94.4 m/s). The process noise in the time-update step is assumed to have a standard deviation of 5 m/s. An example of the PHD particle filter is given in Figure 1.

A. Typical measurements

Table III lists approximate ranges of values observed for the variables introduced in Sec. V.

TABLE III

APPROXIMATE VALUE RANGES OF BISTATIC RADAR VARIABLES.

Variable	typ. min	typ. max
SNR	12.2 dB	32.5 dB
p_D	0.9418	0.99999
σ_r	3.94 m	1.42 km
$\sigma_{\dot{r}}$	6.278 m/s	6.775 m/s
λ	0.213	0.229
$c(z)$	3.4×10^{-8}	3.6×10^{-8}
ΔR_B	3.33 km	4.31 km

The false alarm parameters result in roughly two false alarms for every three time step iterations of the PHD filter. Within a single time step, the number of false alarms typically ranges from zero to four. Since the $\frac{1}{CPI^2}$ term in (19) dominates in the current scenario, the value of $\sigma_{\dot{r}}$ depends only on the three transmitters being used. Thus, it does not acquire a wide range of values in the simulation.

B. Results with $p_{FA} = 10^{-4}$

We first tried the range and velocity tracker using $1{,}000$ particles and an additional 500 birth particles. However, as seen in Figure 2, the range and velocity tracker did not show a drastic improvement over the range-only tracker. Also, the range and velocity tracker would occasionally fail to detect the second target; whereas, the range-only tracker appeared always to detect both targets.

In an attempt to improve the range and velocity tracker, we doubled the number of particles to $3{,}000$ (i.e., $2{,}000$ propagated and $1{,}000$ birth particles). The tracking results are displayed in Figure 3. The tracking performance of the range-only filter, when used with $3{,}000$ particles, is shown in Figure 4. A close-up of the two are depicted in Figure 5. One can see that, with the additional particles, the range and velocity tracker locates the targets with a tighter track than does the range-only tracker, especially when the targets are located far apart from each other. In Figure 5, it appears that there is a slight bias in the range and velocity tracker's results in locating the first target. However, the results are still within a bistatic range cell, and the bias did not appear on subsequent simulation runs. Figure 6 displays the estimated target velocity values found by the range and velocity filter; they appear to track the actual target velocities.

The $3{,}000$ particle range and velocity tracker detected both targets. However, unlike the range-only tracker, which detected both targets immediately, the range and velocity tracker immediately detected the first target but took a few iterations (latencies of 1 to 18 time steps have been observed) to detect the second target. This should not summarily be considered a flaw in the PHD filter, since we should not expect the tracker to detect a target instantly upon its entry into the FoV. Rather, we would expect a brief data accrual time during which the tracker filters out ghost target ambiguity. This may also, however, be due to a lack of a sufficient number of particles being used.

In terms of detecting the correct number of targets at each time step, the range-only tracker, at first glance, appeared to perform slightly better. For example, it overestimated by one the number of targets in twenty time steps; whereas, the range and velocity tracker once underestimated by two, once overestimated by one, and twenty times underestimated by one. However, the underestimation errors of the range and velocity filter occurred at the beginning of the simulation run during which time the filter was trying to detect both targets; whereas, the overestimation errors in the range-only filter occurred throughout the simulation. Thus, the range and velocity tracker demonstrated more stability in maintaining a correct estimate of the number of targets present.

It must also be pointed out, as seen in Figures 2 and 5, that even though the PHD particle filter correctly tracked the two targets in both the $3{,}000$ particle range and velocity tracker and the range-only tracker, it did not correctly extract the target locations at every time step. This was due to the behaviour of the peak-extraction algorithm, which occasionally produced singular covariance matrices or fit two Gaussians to the same peak, thereby locating the

same target twice; whereas, a visual inspection of the PHD filter clearly showed two targets. Increasing the number of particles did ameliorate the peak extraction, since there were more data points available to which to fit the Gaussians. The development of improved peak-extraction algorithms is an important area of PHD research in general; some steps in this direction are suggested in [43].

C. Results with $p_{FA} = 10^{-2}$

The $3{,}000$ particle range-only and range and velocity simulations were performed once more but with $p_{FA} = 10^{-2}$. Since the SNR in the simulations did not change, this increase in probability of false alarm resulted in an increase in p_D, as given by (15). The typical minimum probability of detection, as given in Table III, increased to 0.9978. Within a single time step, the average number of false alarms was 67.

As seen in Figure 7, the range-only tracker could not track the two targets. Furthermore, it was completely unable to estimate the correct number of targets present. At any given time step, it estimated there being between 5 and 31 targets present. On the contrary, the range and velocity tracker was able to track both targets, as shown in Figures 8 and 9. It overestimated the number of targets about 10%-20% of the time (the maximum by which it overestimated was four) and underestimated about 2.5% of the time.

The range and velocity filter with $p_{FA} = 10^{-2}$ did occasionally exhibit behaviour similar to that of the $1{,}500$ particle range and velocity tracker described in Section VI-B. That is, it only tracked the first target, or it tracked the first target for a brief period before dropping it and tracking only the second target for the remainder of the simulation. Other times, it tracked both targets as it should.

VII. Conclusions

A. Importance of High SNR

Initially, the range-only simulation was run using a noise figure of 45 dB to explore a worst-case scenario. However, this was found to be an inappropriate model of the Washington D.C. scenario, since it produced an SNR that was too low over most of the 80 km $\times$ 80 km coverage area. With such poor SNR, the p_D was only above 0.9 for the immediate area around the antenna pairs, while most of the FoV had a p_D close to zero.

The prevalence of low p_D caused the filter to considerably overestimate the number of targets present. Because the birth particles that were added to the filter in the time-update

step were located in an area of low p_D, the filter predicted many targets that did not exist. This is logical, since the filter can only assume that targets are appearing in the area of low SNR based on the birth particle model. It does not receive any radar observation information to contradict the assumption.

We conjecture that restricting birth particle placement to regions of high SNR, or simply restricting the FoV to include only regions of sufficiently high SNR, will mitigate the effect of areas of low p_D on the filter.

B. The PHD Particle Filter

Incorporating Doppler measurements into the PHD-based particle filter was expected to improve the tracking ability of the filter, since the filter would possess additional information about the targets being tracked. The introduction of Doppler measurements, however, while providing additional velocity information, also enlarged the discrepancy between the proposal density used by the particle filter and the true posterior PHD. In the $p_{FA} = 10^{-4}$ case, to achieve at least an equivalent tracking and ghost-busting performance as that of the range-only filter, the number of particles had to be increased, thus increasing the runtime of the tracking system. Once this change was made, however, the tracking performance did improve, as evidenced in Figures 3, 4 and 5. Alternatively, and this remains to be implemented in future work, one could devise a cleverer proposal density that accounts for observed range ellipses when propagating particles in the time-update step, rather than simply use the prior. When using a suboptimal filter – and a particle filter with a finite number of particles is necessarily suboptimal – exploiting more data may require more computation, or at least more sophisticated computation. Several approaches for designing a better proposal density are discussed in [44].

In the $p_{FA} = 10^{-2}$ case, including Doppler information allowed the filter to estimate the correct target number and track the targets, which it could not do with just the range-only measurements. However, since the simulation did not always consistently track both targets, a cleverer proposal density would still be expected to improve tracking performance also in this case. All in all, the PHD filter was effectively able to incorporate the velocity observations and facilitate improved multitarget tracking performance and better target number estimation, but it appears that, in general, this will require either additional particles or increased computation.

It merits a brief mention that the EM algorithm used is the largest consumer of simulation time in our multitarget tracker. With an alternative peak-extraction algorithm, one may be

able to add the additional computation needed to achieve better performance but still retain reasonable computational efficiency.

Another nice avenue for future work would be to compare the PHD-based particle filter to other multitarget tracking methods in the passive radar context. Since the difficulty of peak extraction is a considerable hurdle to jump, the PHD is not so much a multitarget tracking technique as it is an easy multisensor fusion technique in the multitarget context. The PHD is appealing in that it would easily allow us to incorporate other types of measurements, such as angle measurements from an infrared search-and-track sensor or hyperbolic measurements from a time-difference-of-arrival electronic-support-measure (ESM) sensor, into the multitarget tracker. As was the case with velocity measurements, provided we have sufficient computing power, we would expect these additional measurements to improve the multitarget tracker's performance.

ACKNOWLEDGMENTS

This work was enabled via startup funds from the School of Electrical Engineering at the Georgia Institute of Technology, the Demetrius T. Paris Junior Professorship, U.S. Air Force Office of Scientific Research grant F49620-03-1-0340 and the support of Dr. Paul Howland and Dr. Rene van der Heiden of NATO C3 Agency. We thank Dr. Ronald Mahler of Lockheed Martin MS2 Tactical Systems for all the help he has provided us in our work with the Probability Hypothesis Density. We also thank Dr. Raviv Raich for his invaluable review of this paper.

Aaron Lanterman would like to express gratitude to members of the passive radar group at Lockheed Martin Mission Systems, with whom he had the pleasure of interacting while a postdoctoral researcher at the University of Illinois at Urbana-Champaign.

REFERENCES

[1] R. P. S. Mahler, "'Statistics 101' for multisensor, multitarget data fusion," *Aerospace and Electronic Systems Magazine, IEEE*, vol. 19, no. 1, pp. 53–64, Jan 2004.

[2] R. Mahler, "Multitarget moments and their application to multitarget tracking," in *Proc. of The Workshop on Estimation, Tracking, and Fusion: A Tribute to Yaakov Bar-Shalom*, Monterey, CA, May 2001, pp. 134–166.

[3] R. P. S. Mahler, "Multitarget Bayes filtering via first-order multitarget moments," *IEEE Trans. Aerospace and Electronic Systems*, vol. 39, no. 4, pp. 1152–1178, 2003.

[4] M. Tobias and A. D. Lanterman, "A probability hypothesis density-based multitarget tracker using multiple bistatic range and velocity measurements," in *Proc. of the 36th Southeastern Symposium on System Theory*, Atlanta, GA, March 2004, pp. 205–209.

[5] ——, "Multitarget tracking using multiple bistatic range measurements with probability hypothesis densities," in *Signal Processing, Sensor Fusion, and Target Recognition XIII*, I. Kadar, Ed., vol. Proc. SPIE 5429, April 2004, pp. 296–305.

[6] E. A. Wan and R. van der Merwe, "The unscented kalman filter," in *Kalman Filtering and Neural Networks*, S. Haykin, Ed. John Wiley and Sons, 2001, ch. 7.

[7] M. Isard and A. Blake, "Condensation – conditional density propagation for visual tracking," *International Journal of Computer Vision*, vol. 29, no. 1, pp. 5–28, 1998.

[8] A. Doucet, N. de Freitas, and N. Gordon, *Sequential Monte Carlo Methods in Practice*. Springer-Verlag, 2001.

[9] S. C. Herman and P. Moulin, "A particle filtering approach to FM-band passive radar tracking and automatic target recognition," in *Proc. IEEE Aerospace Conference*, vol. 4, Big Sky, Montana, March 9-16 2002, pp. 1789–1808.

[10] A. D. Lanterman, "Sampling from multitarget Bayesian posteriors for random sets via jump-diffusion processes," in *Signal Processing, Sensor Fusion, and Target Recognition XII*, I. Kadar, Ed., vol. Proc. SPIE 5096, Orlando, FL, April 2003.

[11] S. S. Blackman, *Multiple Target Tracking with Radar Applications*. Artech House, 1986.

[12] S. S. Blackman and R. F. Popoli, *Design and Analysis of Modern Tracking Systems*. Artech House, 1999.

[13] T. E. Fortmann, Y. Bar-Shalom, and M. Scheffe, "Sonar tracking of multiple targets using joint probabilistic data association," *IEEE Journal of Oceanic Engineering*, vol. 8, no. 3, pp. 173–184, 1983.

[14] S. Deb, M. Yeddanapudi, K. R. Pattipati, and Y. Bar-Shalom, "A generalized S-D assignment algorithm for multisensor-multitarget state estimation," *IEEE Trans. on Aerospace and Electronic Systems*, vol. 33, no. 2, Part 1, pp. 523–538, April 1997.

[15] T. Kirubarajan, Y. Bar-Shalom, and K. R. Pattipati, "Multiassignment for tracking a large number of overlapping objects (and application to fibroblast cells)," *IEEE Trans. on Aerospace and Electronic Systems*, vol. 37, no. 1, pp. 2–21, Jan. 2001.

[16] R. L. Popp, K. R. Pattipati, and Y. Bar-Shalom, "m-best S-D assignment algorithm with application to multitarget tracking," *IEEE Trans. on Aerospace and Electronic Systems*, vol. 37, no. 1, pp. 22–39, Jan. 2001.

[17] T. Kirubarajan, H. Wang, Y. Bar-Shalom, and K. R. Pattipati, "Efficient multisensor fusion using multidimensional data association," *IEEE Trans. on Aerospace and Electronic Systems*, vol. 37, no. 2, pp. 386–400, April 2001.

[18] A. B. Poore and N. Rijavec, "A lagrangian relaxation algorithm for multidimensional assignment problems arising from multitarget tracking," *SIAM Journal on Optimization*, vol. 3, no. 3, pp. 544–563, Aug. 1993.

[19] A. B. Poore and A. J. Robertson, "A new lagrangian relaxation based algorithm for a class of multidimensional assignment problems," *Computational Optimization and Applications*, vol. 8, pp. 129–150, 1997.

[20] E. W. Kamen, "Multiple target tracking based on symmetric measurement equations," *IEEE Trans. on Automatic Control*, vol. 37, pp. 371–374, April 1992.

[21] E. W. Kamen and C. R. Sastry, "Multiple target tracking using products of position measurements," *IEEE Trans. on Aerospace and Electronic Systems*, vol. 29, no. 2, pp. 476–493, 1993.

[22] C. R. Sastry and E. W. Kamen, "SME filter approach to multiple target tracking with radar measurements," *IEE Proc. F: Radar, Sonar, and Navigation*, vol. 140, no. 4, pp. 251–260, August 1993.

[23] E. W. Kamen and J. Su, *Introduction to Optimal Estimation*. Springer Verlag, 1999.

[24] I. R. Goodman, R. P. S. Mahler, and H. T. Nguyen, *Mathematics of Data Fusion*. Kluwer Academic Publishers, 1997.

[25] R. Mahler, "Engineering statistics for multi-object tracking," in *IEEE Workshop on Multi-Object Tracking*, 2001, pp. 53–60.

[26] ——, "An introduction to multisource-multitarget statistics and its applications," Lockheed Martin, Tech. Rep., 2000.

[27] R. Mahler and T. Zajic, "Multitarget filtering using a multitarget first-order moment statistic," in *Signal Processing, Sensor Fusion, and Target Recognition X*, I. Kadar, Ed., vol. Proc. SPIE 4380, 2001, pp. 184–195.

[28] D. Daley and D. Vere-Jones, *An Introduction to the Theory of Point Processes*. Springer-Verlag, 1988.

[29] L. M. Ehrman, "Automated target recognition using passive radar and a coordinated flight model," Master's thesis, Georgia Institute of Technology, Atlanta, Georgia, May 2004.

[30] A. El-Fallah, T. Zajic, R. Mahler, B. Lajza-Rooks, and R. Mehra, "Multitarget nonlinear filtering based on spectral compression and probability hypothesis density," in *Signal Processing, Sensor Fusion, and Target Recognition X*, I. Kadar, Ed., vol. Proc. SPIE 4380, 2001, pp. 207–216.

[31] R. Mahler, "Objective functions for Bayesian control-theoretic sensor management, I: Multitarget first-moment approximation," in *Proc. of IEEE Aerospace Conference*, vol. 4, Big Sky, MT, March 2003, pp. 1905–1924.

[32] T. Zajic and R. Mahler, "A particle-systems implementation of the PHD multitarget tracking filter," in *Signal Processing, Sensor Fusion, and Target Recognition XII*, I. Kadar, Ed., vol. Proc. SPIE 5096, 2003, pp. 291–299.

[33] B. Vo, S. Singh, and A. Doucet, "Sequential Monte Carlo implementation of the PHD filter for multi-target tracking," in *Proc. FUSION 2003*, Cairns, Australia, 2003, pp. 792–799.

[34] R. P. Mahler, Private e-mail communication, March 11, 2004.

[35] J. A. Bilmes, "A gentle tutorial of the EM algorithm and its application to parameter estimation for Gaussian mixture and hidden markov models," International Computer Science Institute, Berkeley, CA, Tech. Rep. TR-97-021, April 1998.

[36] C. Biernacki, G. Celeux, and G. Govaert, "Choosing starting values for the EM algorithm for getting the highest likelihood in multivariate gaussian mixture models," *Computational Statistics and Data Analysis*, vol. 41, pp. 561–575, Jan. 2003.

[37] M. A. T. Figueiredo, J. M. N. Leitao, and A. K. Jain, "On fitting mixture models," in *Energy Minimization Methods in Computer Vision and Pattern Recognition*, E. Hancock and M. Pellilo, Eds. Springer-Verlag, 1999, pp. 54–69.

[38] N. Willis, *Bistatic Radar*. Technology Service Corporation, 1995.

[39] P. E. Howland, "Television based bistatic radar," Ph.D. dissertation, University of Birmingham, ENGLAND, 1997.

[40] ——, "Target tracking using television-based bistatic radar," *IEE Proc. F: Radar, Sonar, and Navigation*, vol. 146, no. 3, pp. 166–174, June 1999.

[41] B. Mahafza, *Introduction to Radar Analysis*. CRC Press LLC, 1998.

[42] D. Barton, *Modern Radar System Analysis*. Artech House, Inc., 1988.

[43] L. Lin, Y. Bar-Shalom, and T. Kirubarajan, "Data association combined with the probability hypothesis density filter for multitarget tracking," in *Signal and Data Processing of Small Targets 2004*, O. E. Drummond, Ed., vol. Proc. SPIE 5428, April 2004.

[44] A. Doucet, S. Godsill, and C. Andrieu, "On sequential Monte Carlo sampling methods for Bayesian filtering," *Statistics and Computing*, vol. 10, no. 3, pp. 197–208, July 2000.

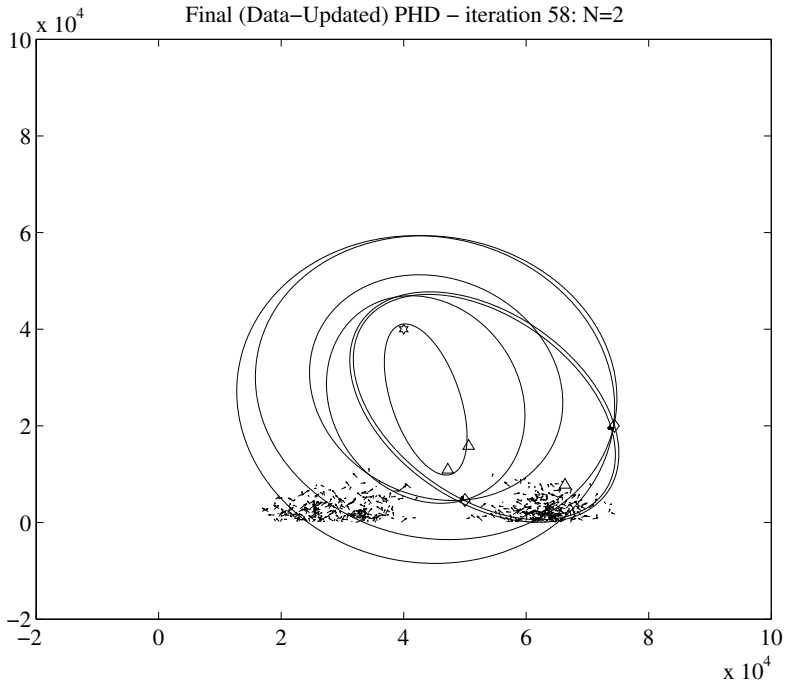

(a) The PHD particle filter and range ellipses. The receiving antenna is represented by the hexagon, and transmitting antennas by the triangles. The two diamonds indicate the actual target positions. Each particle of the filter is pictured. Note the targeted cluster placement of birth particles and the absence of persistent ghost targets.

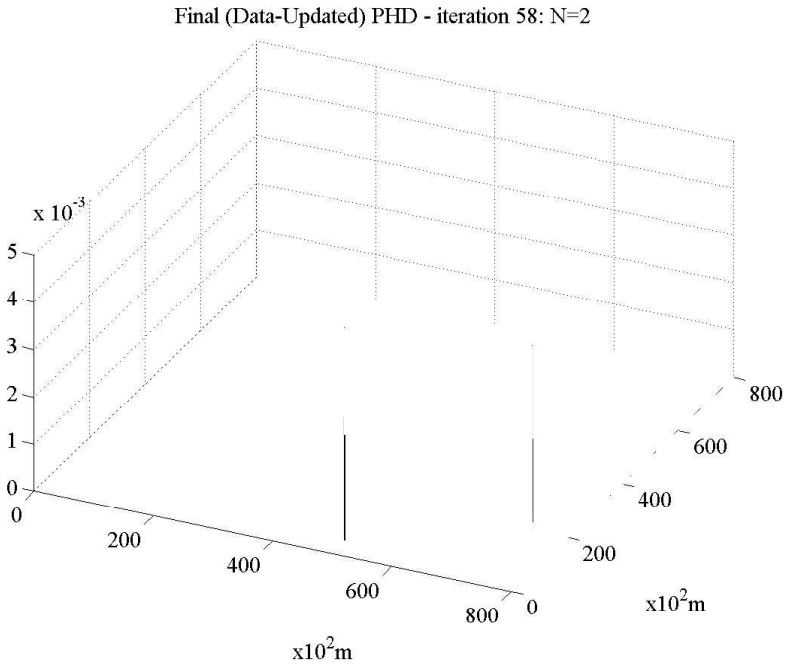

(b) The particle weights of the PHD filter. The sum of the weights is 1.999.

Fig. 1. The $1{,}500$ particle range and velocity PHD filter at time $k = 58$.

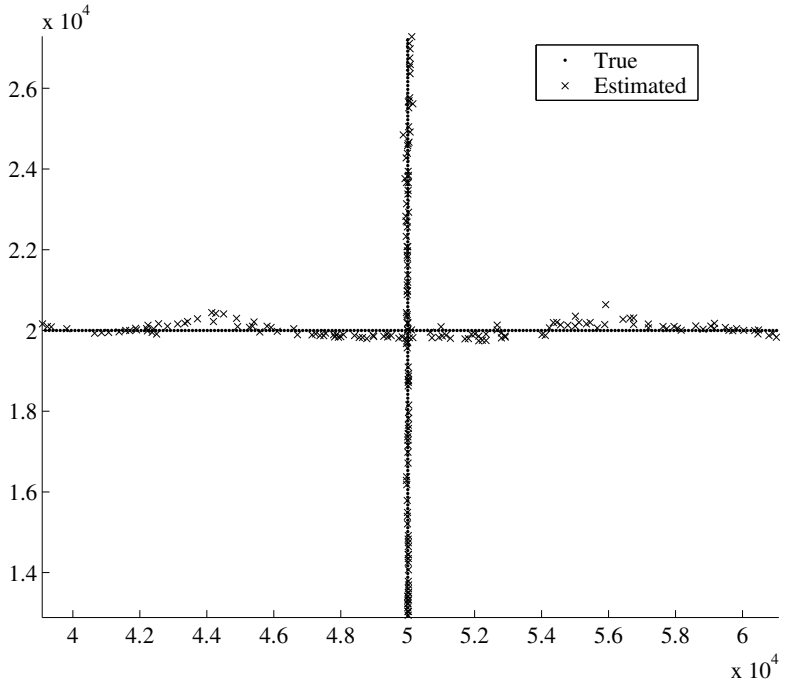

(a) Range and velocity particle filter

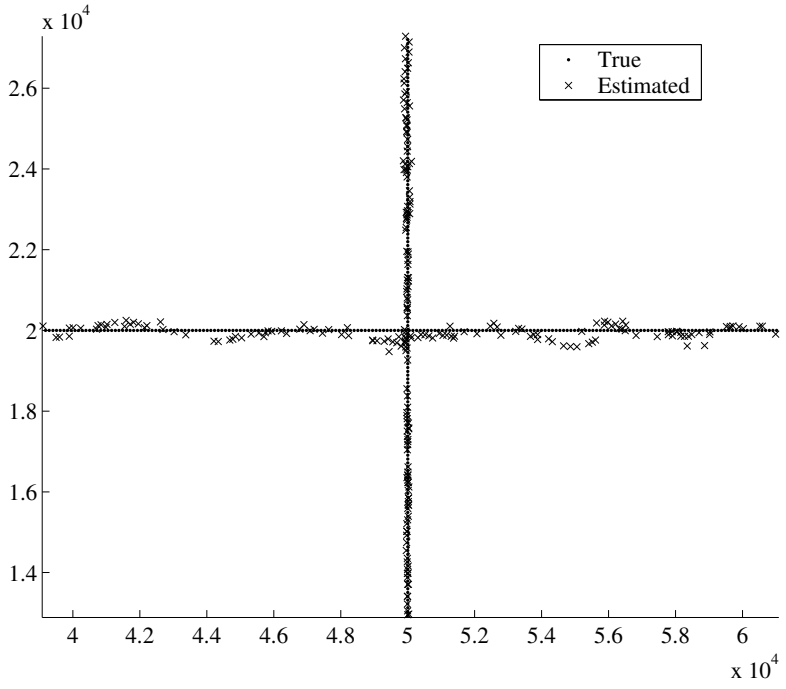

(b) Range-only particle filter

Fig. 2. Close-up of range-only filter results and range and velocity filter results. Both are using $1{,}500$ particles.

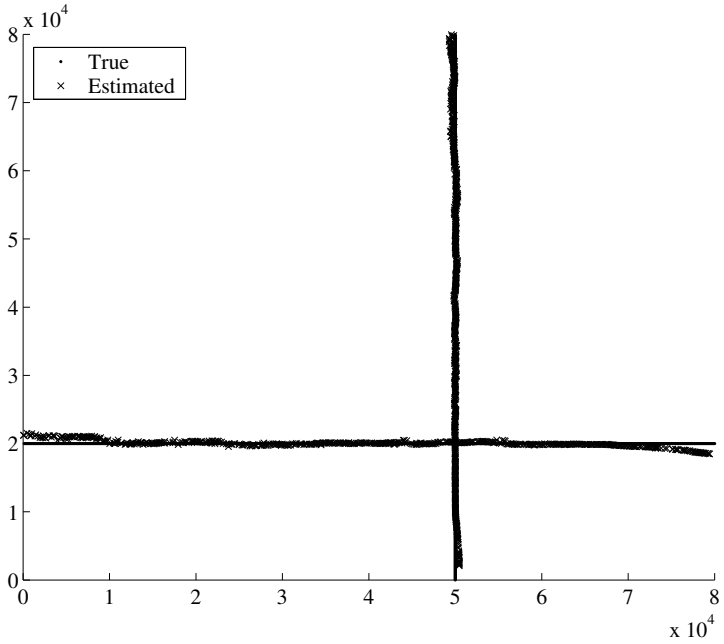

Fig. 3. Actual vs. estimated target locations as given by the 3,000 particle range and velocity PHD filter.

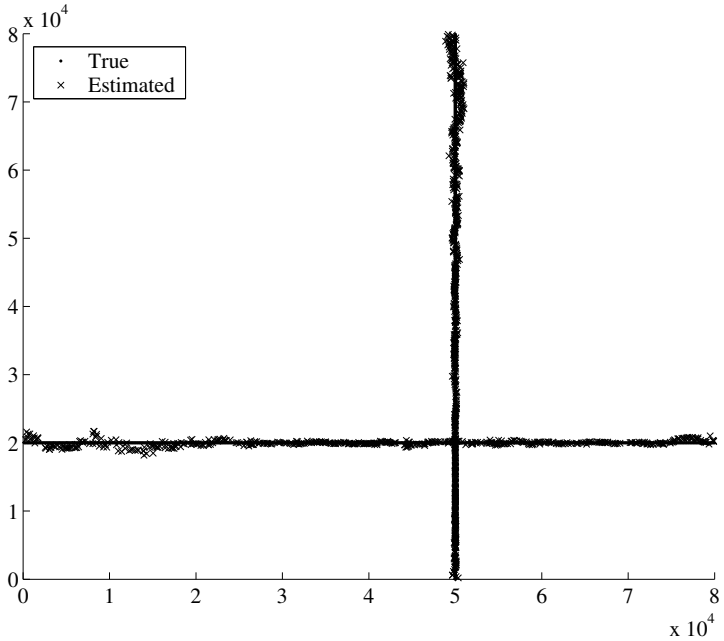

Fig. 4. Actual vs. estimated target locations as given by the 3,000 particle range-only PHD filter.

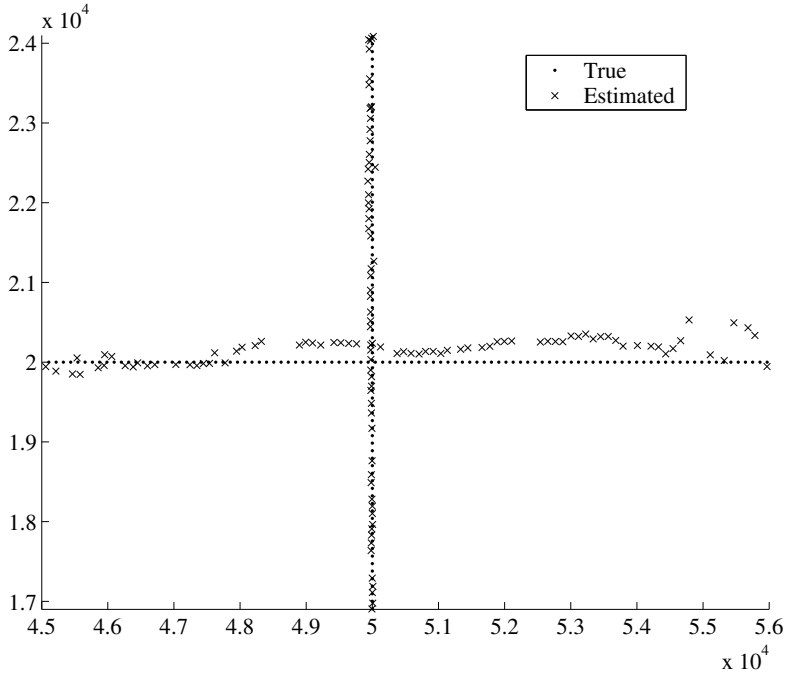

(a) Range and velocity particle filter

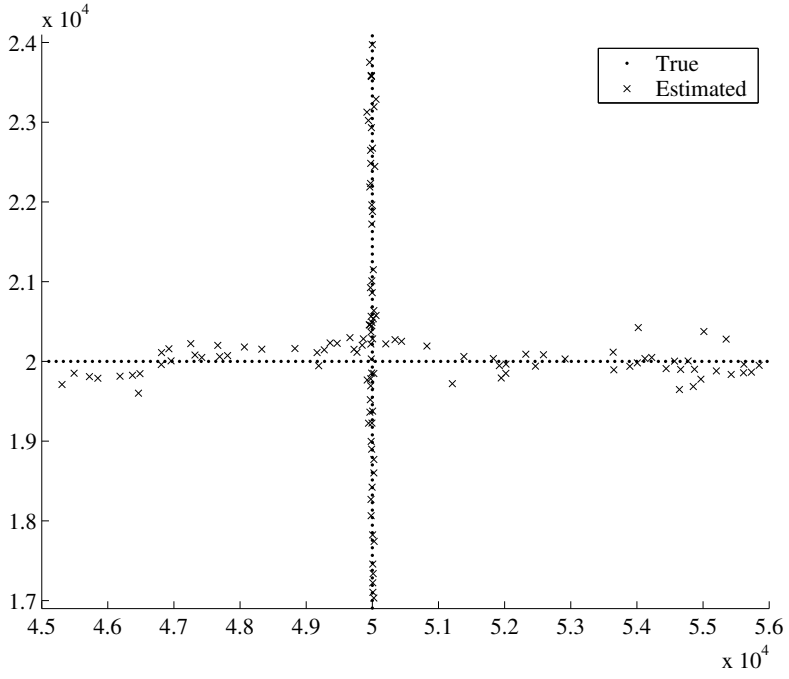

(b) Range-only particle filter

Fig. 5. Close-up of range-only filter results and range and velocity filter results. Both are using 3,000 particles.

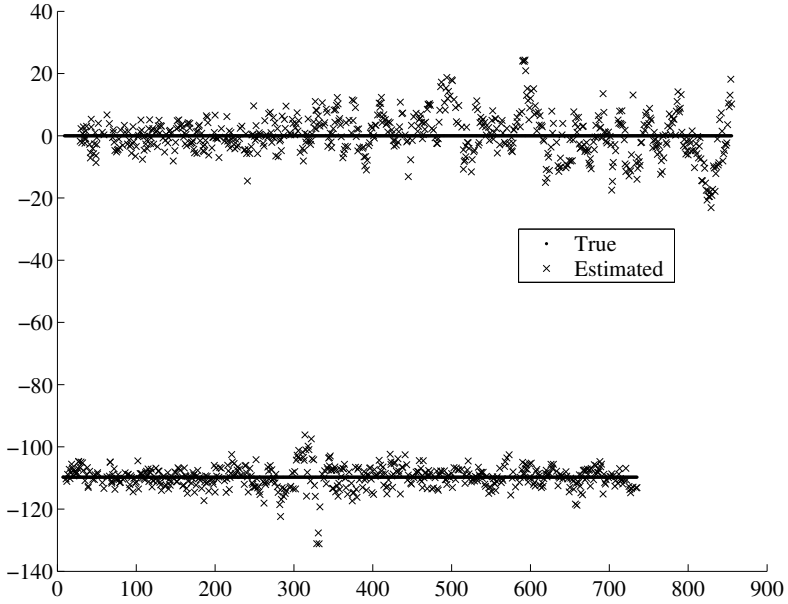

(a) Target $\dot{x}$ components

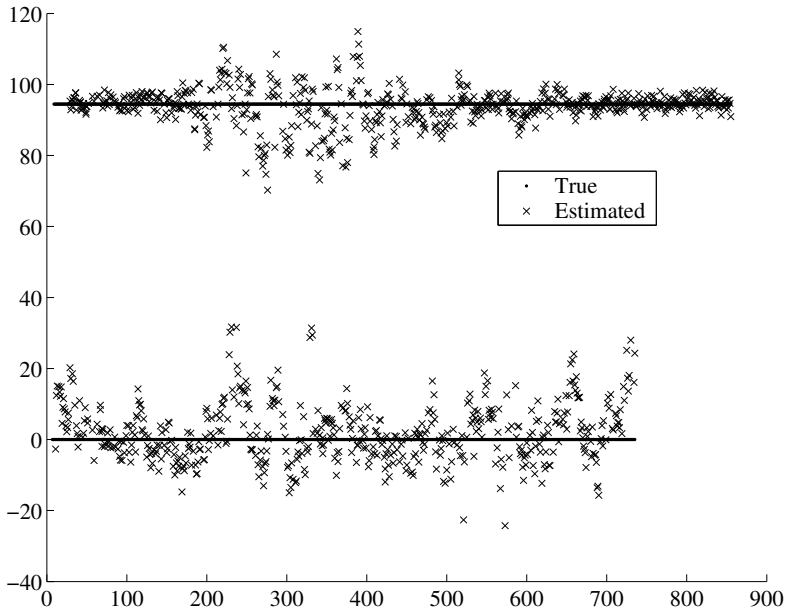

(b) Target $\dot{y}$ components

Fig. 6. Actual vs. estimated target velocities as given by the $3{,}000$ particle range and velocity PHD filter.

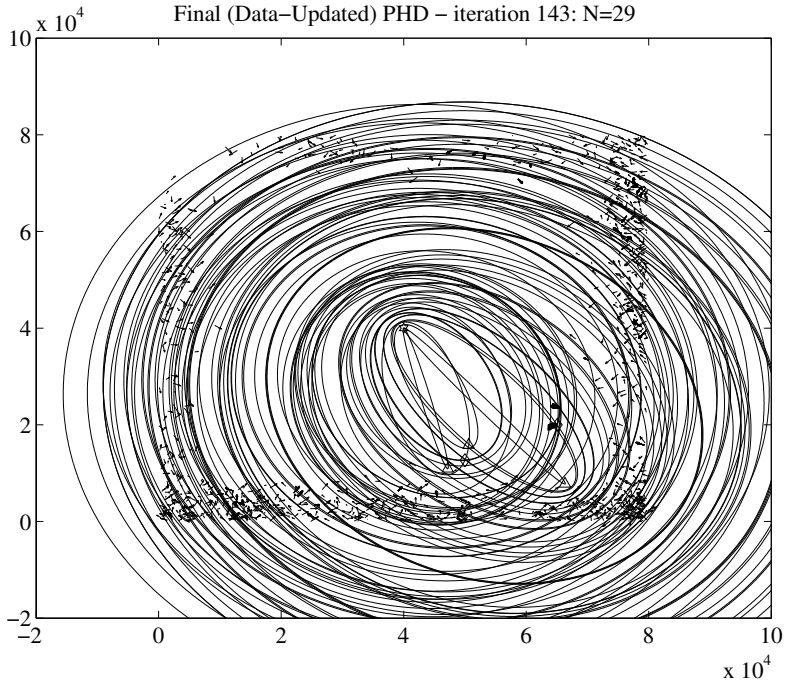

(a) The PHD particle filter and range ellipses. The receiving antenna is represented by the hexagon, and transmitting antennas by the triangles. The two diamonds indicate the actual target positions. Each particle of the filter is pictured.

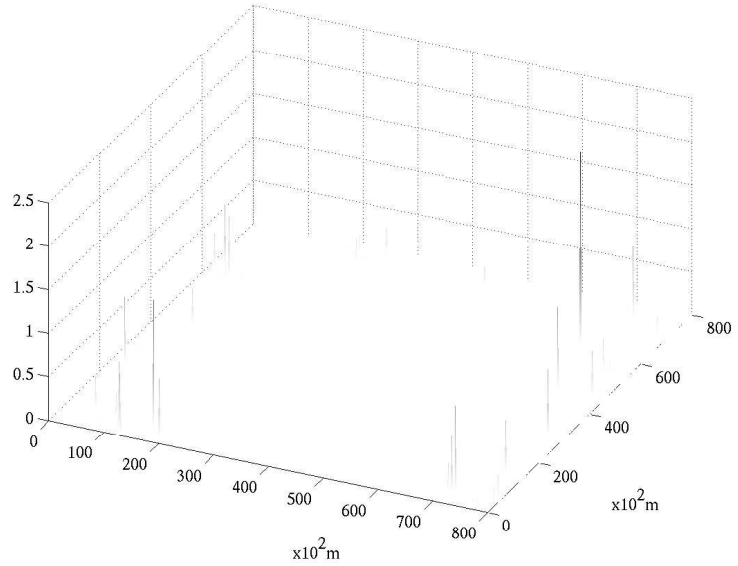

(b) The particle weights of the PHD filter. The sum of the weights is 29.47.

Fig. 7. The 3,000 particle range-only PHD filter at time $k = 143$ when $p_{FA} = 10^{-2}$. There are 81 false alarm observations. The filter estimates 29 targets present.

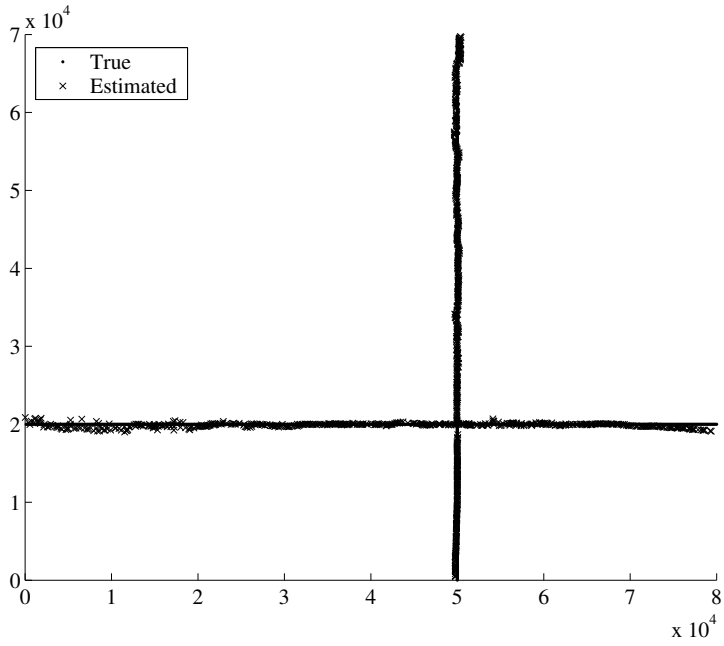

Fig. 8. Actual vs. estimated target locations as given by the 3,000 particle range and velocity PHD filter when $p_{FA} = 10^{-2}$.

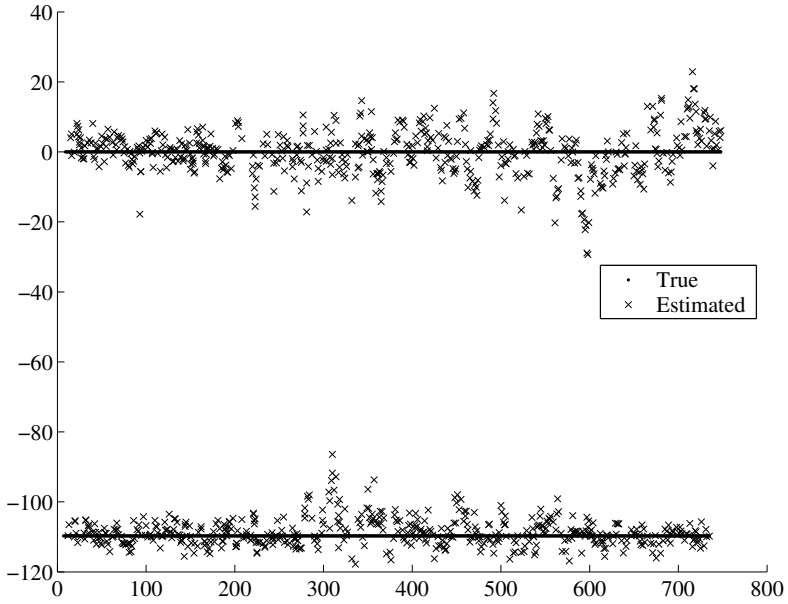

(a) Target $\dot{x}$ components

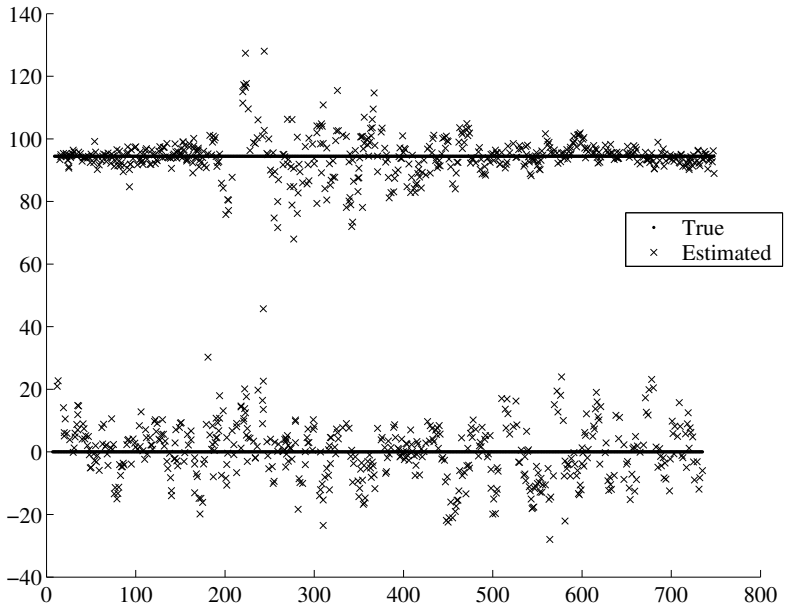

(b) Target $\dot{y}$ components

Fig. 9. Actual vs. estimated target velocities as given by the 3,000 particle range and velocity PHD filter when $p_{FA} = 10^{-2}$.